European Archives of Oto-Rhino-Laryngology
https://doi.org/10.1007/s00405-024-09036-7

OTOLOGY

Erosion of the temporal bone by vestibular schwannoma: morphometrics and predictive modeling

Nicolas Massager[1,2] · Salim El Hadwe[1,3] · Sami Barrit[1] · Mejdeddine Al Barajraji[4] · Daniele Morelli[1] · Cécile Renier[5]

Received: 30 August 2024 / Accepted: 9 October 2024

Abstract

Purpose To perform a comprehensive morphometric analysis of vestibular schwannomas (VS) using multimodal imaging, focusing on the relationship between tumor characteristics and internal acoustic canal (IAC) changes.

Methods We analyzed a cohort of patients undergoing radiosurgery for VS, utilizing high-definition MRI and bone CT for detailed anatomical assessment. Image co-registration and fusion techniques were employed to examine VS and IAC dimensions. Advanced statistical methods, including logistic regression, were applied to identify patterns of IAC dilation and establish predictive indicators for these morphological changes.

Results The study included 659 patients (51.1% female, mean age 56.37 years) with evenly distributed tumor lateralization. Koos grades were I (22.9%), II (29.9%), III (38.2%), IVa (8.9%), and IVb (0.3%). Most tumors (90.9%) extended both inside and outside the IAC. Ipsilateral IAC (IIAC) dimensions were significantly larger than contralateral, with IIAC volume 49% greater ($p < .0001$). Higher Koos grades correlated with increased intra-canalicular lesion volume (icLV), which was strongly associated with IIAC size. Logistic regression identified icLV as the strongest predictor of IIAC dilation (AUC = 0.7674, threshold = 137.52 mm3).

Conclusion The icLV appears central to the pathophysiological development of VS and its impact on IAC anatomy. While limited by a selective patient base and static imaging data, these findings enhance the understanding of VS-IAC interactions, offering insights for improved clinical management and further research.

Keywords Vestibular schwannoma · Bone erosion · Internal auditory canal · Morphometrics · Artificial intelligence · Machine learning

Introduction

Vestibular schwannomas (VS) are benign tumors originating from Schwann cells of the vestibulocochlear nerve, constituting approximately 85% of cerebellopontine angle (CPA) tumors. They can present significant clinical challenges due to their potential to exert substantial mass effects on intracranial structures, despite a low risk of malignant transformation [1].

The phenomenon of bone erosion in the internal auditory canal (IAC) associated with VS has been recognized for decades; however, the underlying pathophysiological mechanisms remain poorly understood [2–5]. This knowledge gap is largely attributed to a scarcity of comprehensive morphometric and radiomic analyses addressing the intricate tumor-bone interactions.

Advancements in imaging technologies now offer deeper insights into the dynamic interplay between VS and

✉ Nicolas Massager
nicolas.massager@ulb.be

Cécile Renier
cecile.renier@chuuclnamur.uclouvain.be

1 Department of Neurological Surgery, CHU Tivoli ULB, Avenue Max Buset 34, 7110 La Louvière, Belgium

2 Faculty of Medicine, Université Libre de Bruxelles, Brussels, Belgium

3 Department of Clinical Neurosciences, University of Cambridge, Cambridge, United Kingdom

4 Department of Neurosurgery, CHUV, Lausanne, Switzerland

5 Department of Radiophysics, CHU UCL Namur-Site Hôpital Sainte-Elisabeth, Namur, Belgium

Published online: 22 October 2024

surrounding bone structures, as well as the natural progression of these tumors [6]. Despite these technological progresses, the specific growth patterns leading to IAC erosion remains elusive. Current evidence suggests that tumor size and growth velocity are pivotal determinants of IAC enlargement, yet there is ongoing debate regarding the exact morphometric predictors responsible for these structural changes [7].

Aligned with the European Association of Neuro-Oncology (EANO) guidelines for VS management [8], this study seeks to elucidate the conditions under which IAC dilation occurs in the context of VS. Hence, we investigated the relationship between morpho-volumetric changes of IAC and VS. By thoroughly assessing tumor-bone interfaces in an extensive cohort with advanced imaging studies and machine learning methods, this research aims to deepen the understanding of the mechanisms driving bone erosion.

Materials and methods

Patient selection

We maintained a single-center prospective database of patients undergoing Gamma Knife radiosurgery (GKRS). All patients treated for a unilateral VS with comprehensive imaging were included. Patients with neurofibromatosis or bilateral VS were excluded.

Imaging acquisition and post-processing

On the same day, each patient underwent a 1-mm thick axial three-dimensional MRI, including both gadolinium-enhanced T1-weighted and T2-weighted sequences without intersectional gaps and a 1-mm thick axial three-dimensional CT scan. We integrated this imaging in the stereotactic planning software Leksell GammaPlan™ (Elekta Instruments®, Sweden) to co-register the CT and MR images, fuse the CT with MR-T1 gadolinium and MR-T2, and perform the volumetrics study.

Structure analysis

All VS were graded according to Koos classification: I (confined to IAC), II (extending into CPA, no brainstem contact), III (brainstem contact, no compression), IV (brainstem compression and 4th ventricle shift) [9, 10]. According to the proposal of Matthies and Samii [4] we separated the Koos grade 4 into two subgroups: grade IVa (brainstem compression without 4th ventricle displacement) and grade IVb (brainstem compression without 4th ventricle shift). We defined subgroups of VS based on their Koos grades: higher (III and IV) vs. lower (I and II), and their location: (i) entirely outside the IAC, (ii) on both sides of the IAC, and (iii) entirely inside the IAC.

We measured the dimensions of the ipsilateral IAC (IIAC) and contralateral IAC (CIAC), comprising their maximal length (Y-axis) and height (Z-axis). We then performed slice-by-slice manual contouring of both IAC and VS to compute their volumes. By doing so, we segmented intra- and extra-IAC volumes, we further measured and calculated total Lesion Volume (tLV), intra-canalicular lesion volume (icLV), and extracanalicular Lesion Volume (ecLV). For our purpose, we defined the putative enlargement of the IAC in the presence of VS using the IIAC/CIAC ratio as shown in Fig. 1.

Statistical analysis

Categorical variables were presented as counts and percentages, while continuous variables were reported as mean with standard deviation (SD). For inferential analyses, we used parametric and non-parametric tests. The normality assumption was tested before test implementation. For all significant findings, we reported effect sizes and p-values. The significance level was set at $\alpha = 0.05$. All statistical analyses, data visualizations, and machine-learning applications were performed using Python.

A T-test was utilized to compare the icLV between the higher and lower Koos grades. The Mann–Whitney U test was employed to evaluate differences in median IIAC/CIAC ratios across Koos grades. Spearman's rank correlation coefficient (ρ) was calculated to ascertain the monotonic relationship between IIAC volume and tLV within each Koos grade group and, similarly, between the IIAC/CIAC ratio and both the icLV and the tLV.

Pearson's correlation test analyzed the linear relationship between tumor volume within the canal and IAC dimensional alterations. The Kruskal–Wallis test evaluated differences in the IIAC/CIAC ratio among patient subgroups based on VS location regarding the canal. This was complemented by Dunn's post hoc tests for pairwise comparisons between groups.

Volumes threshold

We employed logistic regression to investigate the relationship between icLV and IIAC dilation, aiming to identify a volume threshold for potential canal dilation. Three models were developed: one using icLV as the predictor variable, another using tLV, and a third using icLV/IIAC ratio. In all models, canal dilation (dilated or not) was the binary outcome, with dilation defined as an IIAC/CIAC ratio over 1.

Our dataset was divided into training and testing subsets, using 70% for training and 30% for validation. Each logistic regression model was trained on its respective

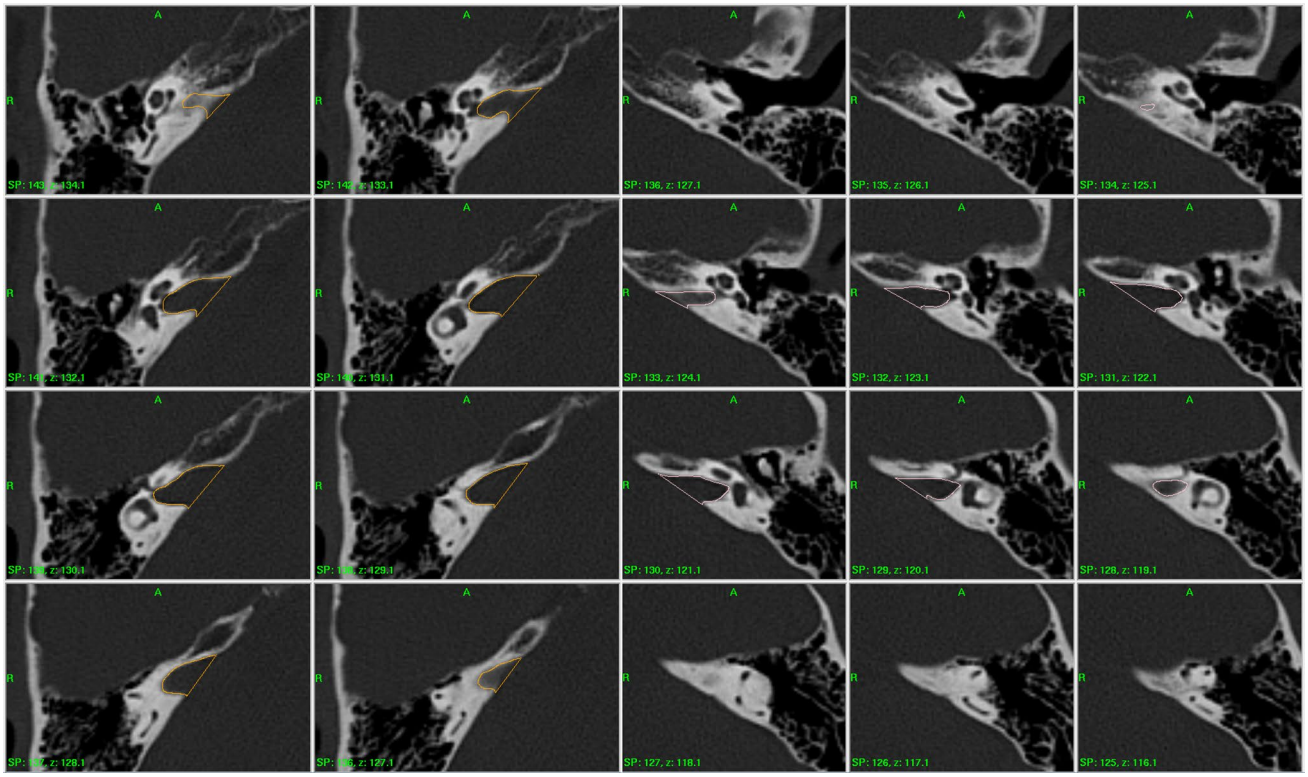

Fig. 1 Methodology of dimension calculation and analysis. This figure illustrates the systematic approach used to calculate the dimensions of each IAC and analyze their correlation with lesion volumetric data. Axial MRI images demonstrate the manual contouring method for measuring, slice-by-slice, the dimensions of the **a** ipsilateral IAC and **b** contralateral IAC. The resulting IIAC/CIAC ratio is applied to assess IAC enlargement due to VS

data to learn the relationship between predictor variables and canal dilation. Model performance was evaluated using the Receiver Operating Characteristic (ROC) curve, and Area Under the Curve (AUC) score was calculated. We identified the optimal canal dilation threshold by finding the point on the ROC curve with the maximum difference between true positive rate (TPR) and false positive rate (FPR). Each model's icLV threshold was calculated using the logistic regression intercept, coefficient, and optimal probability threshold from the ROC analysis. The formula used was: threshold volume = (ln(odds)—intercept) / coefficient, with odds being the ratio of the probability threshold to 1 minus the probability threshold.

Results

The study included a cohort of 659 patients, with a female representation of 51.1% (n = 337). Participant ages ranged from 10.7 to 88.8 years, with a mean of 56.37 years. Table 1 reports the patients' baseline characteristics.

Table 1 Demographic and lesion characteristics of the study cohort

	Total N = 659
Gender	
Males	322 (49.9%)
Females	337 (51.1%)
Age (years)	
Mean	56.37
Range	10.7 – 88.8
Side of the tumor	
Left	337 (51.1%)
Right	322 (49.9%)
Koos grade	
I	151 (22.9%)
II	197 (29.9%)
III	252 (38.2%)
IVa	57 (8.6%)
IVb	2 (0.3%)
Relation of the VS to the IAC	
Outside IAC	15 (2.3%)
Inside IAC	45 (6.8%)
In/outside IAC	599 (90.9%)

IAC internal acoustic canal, *VS* vestibular schwannoma

Lesion characteristics

VS was located on the left in 51.1% of cases (n = 337). The distribution of Koos grades was as follows: 22.9% (n = 151) grade I, 29.9% (n = 197) grade II, 38.2% (n = 252) grade III, 8.6% (n = 57) grade IVa, and 0.3% (n = 2) grade IVb. Most patients, 90.9% (n = 599), exhibited tumors extending both inside and outside the IAC. In contrast, 6.8% (n = 45) had tumors entirely outside the IAC, and 2.3% (n = 15) had tumors entirely within the IAC (Fig. 1).

Dimensions and volumetrics

The IIAC was on average 21% longer than the CIAC (8.4 mm vs. 6.9 mm; $p < 0.0001$), and 35% taller (6.5 mm vs. 4.8 mm; $p < 0.0001$). IIAC volume was 49% larger (294.7 mm3 vs. 197.8 mm3; $p < 0.0001$). The mean tLV was 1501.83 mm3, icLV was 177.04 mm3, and ecLV was 1324.79 mm3. Table 2 details these results.

Koos grade analysis and correlations

Patients with higher Koos grades had significantly larger mean icLV (214.97 mm3 vs. 143.14 mm3, $p = 1.403e-11$). They also had a significantly higher median IIAC/CIAC ratio ($p = 7.564e-24$). A significant positive correlation between IIAC volume and tLV was found in lower Koos grades ($\rho = 0.412$, $p = 5.188e-26$), but not in higher grades ($\rho = 0.023$, $p = 8.634e-01$)(Figs. 2, 3).

IIAC/CIAC analysis and correlations

Significant correlations were found between the IIAC/CIAC ratio and icLV ($\rho = 0.532$, $p < 0.0001$), and between the IIAC/CIAC ratio and tLV ($\rho = 0.473$, $p < 0.0001$).

Table 2 Comparison of ipsilateral and contralateral internal acoustic canal metrics

IAC Metric		IIAC	CIAC	I/C ratio	p-value
Diameter (mm)	Mean (SD)	8.4 (2.1)	6.9 (1.5)	1.2 (0.3)	< 0.0001
	Range	4.4–17.4	3.6–15.0	–	–
Height (mm)	Mean (SD)	6.5 (2.1)	4.8 (1.2)	1.4 (0.5)	< 0.0001
	Range	1.4–16.1	1.7–10.6	–	–-
Volume (mm3)	Mean (SD)	294.7 (150.6)	197.8 (65.4)	1.5 (0.6)	< 0.0001
	Range	78.4–1850	60.9–421.3	0.6–7.5	–

IAC internal acoustic canal, *IIAC* ipsilateral IAC, *CIAC* contralateral IAC

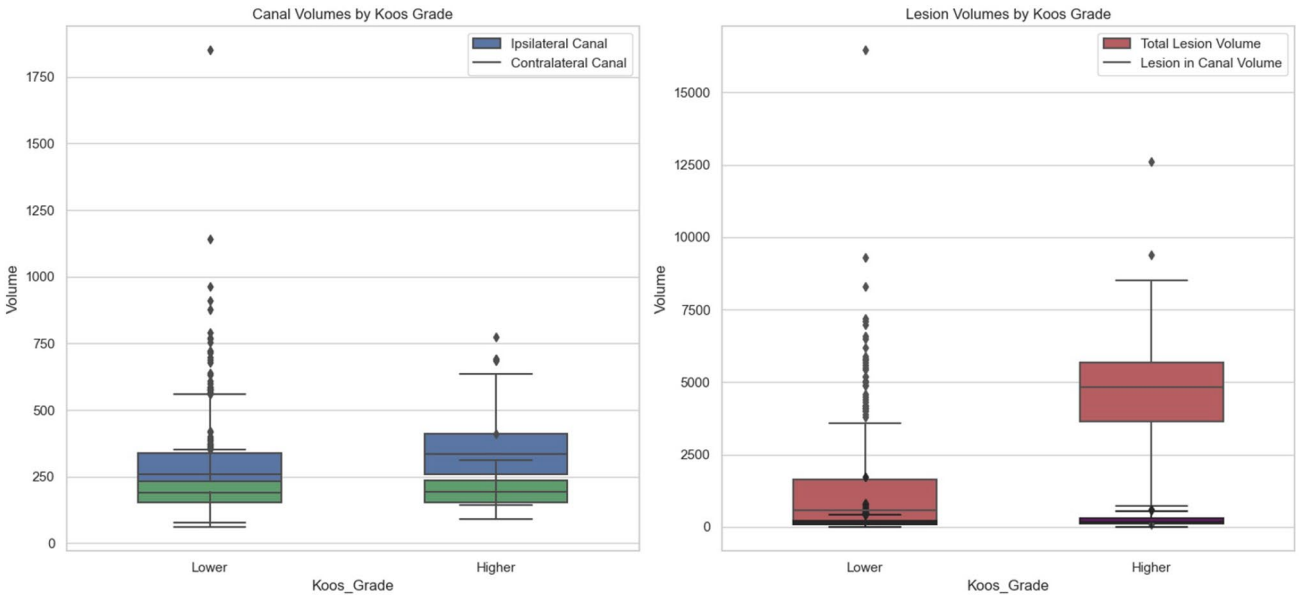

Fig. 2 Comparative analysis of canal and lesion volumes by Koos Grade. This figure presents a comparative box plot analysis, delineating the volume distributions of the ipsilateral and contralateral internal acoustic canals (left panel) and the total lesion volume versus lesion volume within the canal (right panel), stratified by lower and higher Koos grades. The box plots illustrate the median, interquartile range, and outliers, offering a visual representation of the volumetric differences and the spread of measurements within each category

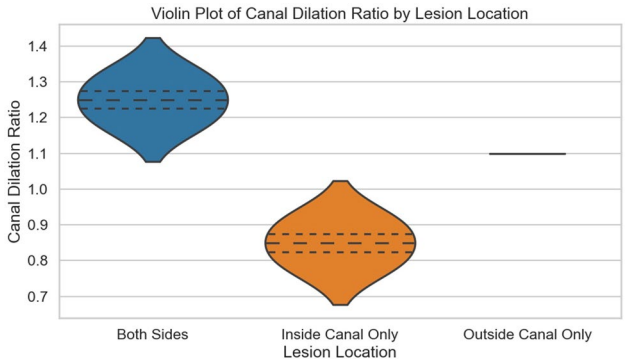

Fig. 3 Violin Plot Illustrating Canal Dilation Ratios by Lesion Location. This figure features a violin plot that provides a visual comparison of the canal dilation ratio across different lesion locations: lesions affecting both sides of the IAC, lesions confined within the canal, and lesions located exclusively outside the canal. Each violin plot encapsulates the distribution density of the ratios, with the width representing the frequency of data points at different ratio levels. The plot distinctly showcases the median, interquartile range, and the full range of canal dilation ratios for each lesion location group, highlighting the variability and skewness of the ratios associated with the lesion location within the IAC

Correlation of dimensions with lesion volumetric data

Positive correlations were found between icLV and IIAC dimensions: length ($r = 0.622$, $p < 0.0001$), height ($r = 0.617$, $p < 0.0001$), and volume ($r = 0.874$, $p < 0.0001$). For tLV, moderate correlations were observed: length ($r = 0.304$, $p < 0.0001$), height ($r = 0.325$, $p < 0.0001$), and volume ($r = 0.229$, $p < 0.0001$).

Cutoff determination

We evaluated three logistic regression models to predict IIAC dilation using lesion volumes.

The first model, incorporating icLV as the predictor, showed superior efficacy and was reported. The model's AUC was 0.7674 (Fig. 4). The regression analysis revealed an intercept of 0.6609 and an icLV coefficient of 0.0092. The model's Pseudo R-squared value was 0.09469 with a log-likelihood of –156.14. The calculated threshold volume for canal dilation was 137.52 mm^3 (Fig. 5). Additional models are in the supplementary information.

Subgroup analysis

Group-wise analysis of VS location relative to the canal showed significant variations in the IIAC/CIAC ratio ($H = 30.621$, $p = 2.242 \times 10 - 7$). Dunn's post hoc tests found no significant difference in canal dilation ratios between intracanal-only and extracanal-only lesions ($p = 0.943421$). However, significant differences were found between intracanal-only and both-side lesions ($p = 1.00 \times 10 - 6$) and between extracanal-only and both-side lesions ($p = 0.005022$).

Subgroup analysis of patients with larger contralateral canal

We analyzed 89 patients with a larger CIAC than IIAC; age and gender distribution did not significantly differ from the other group ($U = 28{,}231.0$, $p = 0.086$ and $Chi^2 = 8.65 \times 10 - 6$, $p = 0.998$). Tumor grading showed more patients in lower Koos grades (40 in grade I and 33

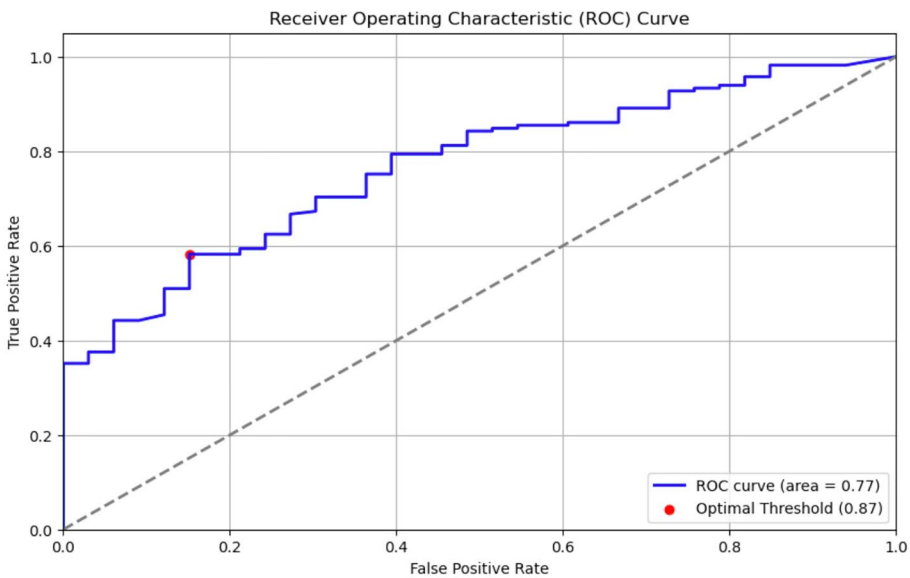

Fig. 4 Receiver Operating Characteristic (ROC) Curve for Intracanal Lesion Volume Model. The ROC curve displays the true positive rate versus the false positive rate for the logistic regression model predicting canal dilation based on intracanal lesion volume. The area under the curve (AUC) is 0.77. The red dot indicates the optimal threshold, where the sum of sensitivity and specificity is maximized

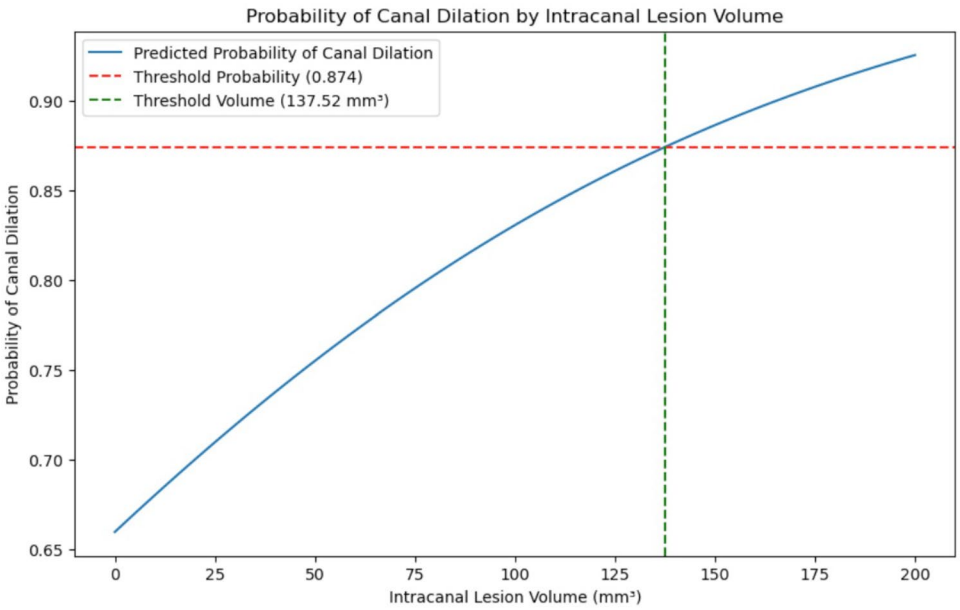

Fig. 5 Probability of Canal Dilation by Intracanal Lesion Volume. This graph delineates the predicted probability of canal dilation as a function of intracanal lesion volume. The solid blue line represents the logistic regression model's predicted probabilities, with the red dashed line indicating the threshold probability above which canal dilation is likely. The green dashed line marks the identified threshold volume of 137.52 mm3, where the probability of canal dilation notably increases, serving as a potential clinical reference point for intervention

in grade II), while the typical group had a broader distribution ($Chi^2 = 42.227$, $p = 1.497 \times 10 - 8$).

Discussion

Summary of findings

This study analyzed 659 individuals undergoing stereotactic radiosurgery for cerebellopontine angle lesions consistent with VS. The cohort had a slight female predominance, ages ranging from 10.7 to 88.8 years (mean age 56.37), with about half of the lesions left-sided and most classified as Koos grade III. The analysis showed significant differences in dimensions and volumes between the IIAC and CIAC, with IIAC being larger across all parameters. This was especially notable considering the wide range of tLV among patients. Higher Koos grades correlated with increased icLV. However, it was the correlation between the IIAC/CIAC ratio and lesion volumes that highlighted how tumor size and location affect canal dimensions, differing notably between lower and higher Koos grades. A logistic regression model pinpointed an icLV threshold of 137.52 mm3, beyond which canal enlargement is likely, suggesting a candidate quantitative marker for clinical decision-making. The study also observed varied enlargement ratios based on tumor localization, contributing to the nuanced understanding of lesion impact. Subgroup analysis showed patients with larger contralateral canals had similar age and gender to the main group but tended to have lower Koos grades.

Bony erosion of IIAC and location of the VS

In the era preceding widespread MRI use, radiological signs of IIAC enlargement, particularly compared to the contralateral side, often suggested VS presence[11, 12]. Despite this longstanding observation, comprehensive empirical evidence elucidating the direct correlation between VS characteristics and IIAC dilation has been limited[4]. Moreover, the specific pathophysiological underpinnings have yet to be fully elucidated.

Our investigation provides compelling evidence supporting a strong association between VS presence and IIAC enlargement, implicating tumor growth as a principal factor in bony erosion. Although similar findings have been reported in previous studies[4, 5, 13, 14], the breadth of our cohort offers a robust dataset that substantiates this correlation more concretely.

Furthermore, we investigate the relationship between lesion size at diagnosis—a factor often correlated with the emergence of clinical symptoms such as hypoacousis, tinnitus, and vestibular disturbances—and IIAC enlargement. Our analysis reveals significant variability in how the tumor's location relative to the IAC influences canal dilation. Notably, the data suggest a direct correlation between larger tumor volumes and more pronounced IIAC enlargement. However, it is the icLV that exhibits a stronger statistical correlation with IIAC dilation, as evidenced by the machine learning models applied in our study (Supplemental information).

This finding could have clinical implications, especially in enhancing the prognostic accuracy for VS management. The critical decision to pursue active treatment versus a

conservative 'Wait and Scan' strategy remains a pivotal challenge[1, 15]. In this context, easily accessible metrics, such as tumor size and volume, IIAC dimensions, and the tumor's intracanalicular proportion, become invaluable. Our results suggest these parameters could be refined and integrated into decision-making algorithms to optimize the management strategies for patients with VS.

Putative etiology of symptoms associated with VS expansion

Despite considerable research, the mechanisms underlying hearing loss in patients with VS remain puzzling. Various hypotheses have been proposed, including direct compression of the auditory nerve by the tumor and vascular insufficiency in the inner ear[13], elevated pressure within the IAC due to tumor extension[16], and the presence of tumor-secreted immune-related biomarkers in plasma[17].

Our investigation contributes by supporting a clear correlation between icLV and IIAC expansion via a mechanism of bony erosion. This association suggests that increased intracanalicular pressure, driven by tumor enlargement within the IAC, likely facilitates the dimensional changes we observe. Consequently, our findings bolster elevated intracanalicular pressure as a contributory factor to hearing loss in this patient population, marking a significant step forward in our comprehension of VS-associated auditory impairment's pathophysiological underpinnings.

Moreover, this study goes a step further, attempting to identify a precise icLV threshold that initiates the dilation of the IIAC. Through logistic regression analysis, we identified a critical volume threshold—137.52 mm^3—at which point canal expansion becomes probable. It is crucial to acknowledge, however, the complexity inherent in these relationships. While our models shed light on this dynamic, the inconsistency in reliability across different models underscores the multifaceted nature of VS pathophysiology. Consequently, our analysis points to a broader landscape of factors beyond icLV that warrants deeper exploration.

Future directions

This study uses logistic regression, a common machine-learning technique, to explore the relationship between icLV and IAC dilation. This threshold correlates with tumor size and clinical outcomes[18], providing a useful metric for treatment decisions. However, the linear assumptions of logistic regression between predictors and the log odds of the outcome may oversimplify the complex, non-linear interactions in tumor progression and IAC changes[19, 20]. The inconsistency in model reliability across different analyses further underscores the multifaceted nature of VS pathophysiology. Future research could benefit from more sophisticated models—e.g. support vector machines, random forests, and neural networks—to capture non-linear patterns and interactions among a broader range of features, including radiomic data, patient demographics, and temporal dynamics of tumor growth[21, 22]. Such advanced methods could enhance risk stratification, offering more nuanced and accurate predictions of clinical outcomes[23]. Incorporating temporal models, such as recurrent neural networks, could further improve predictive performance by accounting for longitudinal changes in tumor size and IAC morphology, potentially enabling real-time adaptive models that refine predictions as new data becomes available[24, 25]. While our logistic regression approach has yielded valuable insights, these advanced techniques could significantly broaden the scope and precision of predictive modeling in VS management.

Limitations

While our study provides valuable insights into the anatomical alterations within the bilateral IAC's among VS patients, as delineated by high-definition radiological imaging, it is imperative to acknowledge its limitations. Primarily, our cohort consisted solely of patients undergoing GKRS. This selection criterion may introduce bias, as it does not encompass newly diagnosed patients or those opting for or eligible for alternative treatments. However, the collected data analyzed in this study have not been influenced in any way by this treatment strategy, since the data have been collected before radiosurgical irradiation. The disadvantage of this cohort selection is that it could potentially limit the generalizability of our findings across the wider spectrum of individuals with VS. On the other hand, this cohort included only patients with a formal treatment indication, which offers a much more significant interest of the role of bone erosion for patients with VS since it provides information when treatment is needed.

Given that our cohort was non-surgical, diagnoses were based on radiological findings without histopathological confirmation. Although contemporary imaging techniques offer high diagnostic accuracy, they do not provide the definitive pathognomonic confirmation that histopathology ensures.

The reliance on static imaging data in this study provides only a snapshot of the condition, without capturing the dynamic progression of VS over time. This cross-sectional design restricts our ability to investigate the disease's evolution.

Recognizing these limitations emphasizes the need for studies with more diverse patient cohorts, encompassing various treatment modalities, and employing longitudinal designs to monitor the temporal dynamics of VS. Integrating

detailed clinical outcomes, including symptomatology and neurological function, with our radiological observations will be crucial for deepening our understanding of VS and improving patient care strategies.

Conclusions

This study offers a comprehensive morphometric analysis of VS and their impact on IAC anatomy in a large cohort of patients treated with GKRS. The icLV emerged as a key predictor of IAC dilation, highlighting its potential as a marker for assessing bony erosion and disease progression.

The identification of a critical icLV threshold for canal dilation provides a quantitative tool that could improve clinical decision-making, particularly in distinguishing between patients requiring active intervention versus conservative management. Additionally, the variability in canal dimensions based on tumor location offers insights into the spatial dynamics of VS growth and its clinical implications.

Despite the study's limitations, including its focus on a radiosurgery-treated cohort and static imaging data, these findings enhance the understanding of VS pathophysiology. Future research should validate these results in more diverse populations and incorporate longitudinal data to better capture VS progression, ultimately refining treatment strategies and improving patient care.

Supplementary Information The online version contains supplementary material available at https://doi.org/10.1007/s00405-024-09036-7.

Author contributions N. Massager: design, acquisition of data, data analysis & interpretation, drafting, final approval, and accountability for the work; final approval of the version to be published; agreement to be accountable for all aspects of the work in ensuring that questions related to the accuracy or integrity of any part of the work are appropriately investigated and resolved. S. El Hadwe: design, acquisition of data, data analysis & interpretation, drafting, final approval, and accountability for the work; final approval of the version to be published; agreement to be accountable for all aspects of the work in ensuring that questions related to the accuracy or integrity of any part of the work are appropriately investigated and resolved. S. Barrit; M. Al Barajraji; D. Morelli; C. Renier: design, data analysis & interpretation, revising the manuscript for important intellectual content.

Funding The authors declare no source of funding.

Data availability All data generated or analyzed during this study are included in this article. Further inquiries can be directed to the corresponding author.

Declarations

Conflict of interest The authors have no conflicts of interest to declare.

Ethical approval The World Medical Association Declaration of Helsinki conducted the current research ethically. The patients have given their written informed consent. The study protocol was approved by the institute's committee on human research (ref. P2015/207).

Informed consent Not required.

References

1. Gupta VK, Thakker A, Gupta KK (2020) Vestibular schwannoma: what we know and where we are heading. Head Neck Pathol 14(4):1058–1066. https://doi.org/10.1007/s12105-020-01155-x
2. Smirniotopoulos JG, Yue NC, Rushing EJ (1993) Cerebellopontine angle masses: radiologic-pathologic correlation. Radiographics 13(5):1131–1147. https://doi.org/10.1148/radiographics.13.5.8210595
3. Takada Y, Ohno K, Hirakawa K (1996) Morphological and clinical study of acoustic tumor with respect to enlargement of internal auditory canal: mechanism of bone destruction. No Shinkei Geka 24(8):739–742
4. Matthies C, Samii M, Krebs S (1997) Management of vestibular schwannomas (acoustic neuromas): radiological features in 202 cases-their value for diagnosis and their predictive importance. Neurosurgery 40(3):469–482. https://doi.org/10.1097/00006123-199703000-00009
5. Tsunoda A, Terasaki O, Muraoka H, Komatsuzaki A, Kimura Y (2001) Cross-sectional shapes of the internal auditory canal in patients with acoustic neuromas. Acta Otolaryngol 121(5):627–631
6. Reznitsky M, Petersen MMBS, West N, Stangerup SE, Cayé-Thomasen P (2021) The natural history of vestibular schwannoma growth—prospective 40-year data from an unselected national cohort. Neuro Oncol 23(5):827–836. https://doi.org/10.1093/neuonc/noaa230
7. Li J, Deng X, Ke D, Cheng J, Zhang S, Hui X (2021) Risk factors for progression in vestibular schwannomas after incomplete resection: a single center retrospective study. Front Neurol. https://doi.org/10.3389/fneur.2021.778590
8. Goldbrunner R, Weller M, Regis J et al (2020) EANO guideline on the diagnosis and treatment of vestibular schwannoma. Neuro Oncol 22(1):31–45. https://doi.org/10.1093/neuonc/noz153
9. Erickson NJ, Schmalz PGR, Agee BS et al (2019) Koos classification of vestibular schwannomas: a reliability study. Neurosurgery 85(3):409–414. https://doi.org/10.1093/neuros/nyy409
10. Wagner F, Gandalini M, Hakim A et al (2018) Radiosurgery of vestibular schwannoma: prognostic factors for hearing outcome using 3D-constructive interference in steady state (3D-CISS). Strahlenther Onkol 194(12):1132–1143. https://doi.org/10.1007/s00066-018-1361-8
11. Valvassori GE (1969) The abnormal internal auditory canal: the diagnosis of acoustic neuroma. Radiology 92(3):449–459. https://doi.org/10.1148/92.3.449
12. Robbins B, Marshall WH (1978) Computed tomography of acoustic neurinoma. Radiology 128(2):367–370. https://doi.org/10.1148/128.2.367
13. Tsunoda AKYA (2000) Three-dimensional imaging of the internal auditory canal in patients with acoustic neuroma. Acta Otolaryngol 120(542):6–8. https://doi.org/10.1080/000164800454576
14. Feghali JG, Kantrowitz AB (1995) Atypical invasion of the temporal bone in vestibular schwannoma. Skull Base Surg 5(1):33–36. https://doi.org/10.1055/s-2008-1058948
15. Kania R, Vérillaud B, Camous D et al (2018) EAONO position statement on vestibular schwannoma: imaging assessment question: how should growth of vestibular schwannoma be defined? J Int Adv Otol 14:90–94. https://doi.org/10.5152/iao.2018.5360
16. Badie B, Pyle GM, Nguyen PH, Hadar EJ (2001) Elevation of internal auditory canal pressure by vestibular schwannomas. Otol

Neurotol 22(5):696–700. https://doi.org/10.1097/00129492-200109000-00024
17. Vasilijic S, Atai NA, Hyakusoku H et al (2023) Identification of immune-related candidate biomarkers in plasma of patients with sporadic vestibular schwannoma. Sci Adv. https://doi.org/10.1126/sciadv.adf7295
18. Hosmer DW, Lemeshow S (2000). Applied logistic regression (2nd ed.). Wiley18. Hosmer, D. W., & Lemeshow, S. (2000). Applied Logistic Regression (2nd ed.). Wiley.
19. Kleinbaum DG, Klein M (2010) Logistic regression: a self-learning text. Springer, Cham
20. Kuhn M, Johnson K (2013) Applied predictive modeling. Springer
21. Breiman L (2001) Random forests. Mach Learn 45(1):5–32. https://doi.org/10.1023/A:1010933404324
22. Vapnik VN (1995) The nature of statistical learning theory. Springer
23. Borzooei S, Briganti G, Golparian M et al (2024) Machine learning for risk stratification of thyroid cancer patients: a 15-year cohort study. Eur Arch Otorhinolaryngol 281:2095–2104. https://doi.org/10.1007/s00405-023-08299-w
24. Hochreiter S, Schmidhuber J (1997) Long short-term memory. Neural Comput 9(8):1735–1780. https://doi.org/10.1162/neco.1997.9.8.1735
25. Das S, Tariq A, Santos T, et al. Recurrent Neural Networks (RNNs): Architectures, training tricks, and introduction to influential research. 2023 Jul 23. In: Colliot O, editor. Machine learning for brain disorders [Internet]. New York, NY: Humana; 2023. Chapter 4. Available from: https://www.ncbi.nlm.nih.gov/books/NBK597502/ https://doi.org/10.1007/978-1-0716-3195-9_4